

Accepted for publication in The Astrophysical Journal

## The Angular Diameter of $\lambda$ Boötis

David R. Ciardi, Gerard T. van Belle, Andrew F. Boden

*Michelson Science Center/Caltech  
770 South Wilson Avenue, M/S 100-22 Pasadena, CA 91125*

ciardi@ipac.caltech.edu

T. ten Brummelaar, H. A. McAlister, W.G. Bagnuolo, Jr.  
P. J. Goldfinger, J. Sturmann, L. Sturmann, N. Turner,

*Center for High Angular Resolution Astronomy, Department of Physics and Astronomy,  
Georgia State University, Atlanta, GA 30302-4106*

D. H. Berger

*University of Michigan, Dept. of Astronomy,  
Ann Arbor, MI 48109-1042*

R. R. Thompson

*Michelson Science Center/Caltech  
770 South Wilson Avenue, M/S 100-22 Pasadena, CA 91125*

and

S. T. Ridgway

*National Optical Astronomy Observatories  
P.O. Box 26732, Tucson, AZ 85726-6732*

### ABSTRACT

Using the CHARA Array and the Palomar Testbed Interferometer, the chemically peculiar star  $\lambda$  Boötis has been spatially resolved. We have measured the limb darkened angular diameter to be  $\theta_{LD} = 0.533 \pm 0.029$  mas, corresponding to a linear radius of  $R_{\star} = 1.70 \pm 0.10 R_{\odot}$ . The measured angular diameter yields an effective temperature for  $\lambda$  Boo of  $T_{eff} = 8887 \pm 242$  K. Based upon literature

surface gravity estimates spanning  $\log(g) = 4.0 - 4.2$  [ $\text{cm s}^{-2}$ ], we have derived a stellar mass range of  $M_\star = 1.1 - 1.7 M_\odot$ . For a given surface gravity, the linear radius uncertainty contributes approximately  $\sigma(M_\star) = 0.1 - 0.2 M_\odot$  to the total mass uncertainty. The uncertainty in the mass (i.e., the range of derived masses) is primarily a result of the uncertainty in the surface gravity. The upper bound of our derived mass range ( $\log(g) = 4.2$ ,  $M_\star = 1.7 \pm 0.2 M_\odot$ ) is consistent with 100 – 300 MYr solar-metallicity evolutionary models. The mid-range of our derived masses ( $\log(g) = 4.1$ ,  $M_\star = 1.3 \pm 0.2 M_\odot$ ) is consistent with 2 – 3 GYr metal-poor evolutionary models. A more definitive surface gravity determination is required to determine a more precise mass for  $\lambda$  Boo.

*Subject headings:* stars – stars: individual ( $\lambda$  Boötis) – stars: fundamental parameters – techniques: interferometric: circumstellar material – infrared

## 1. Introduction

$\lambda$  Boötis stars are a chemically peculiar class of late-B to mid-F stars (Morgan, Keenan, & Kellman 1943). The stars are depleted of heavy elements like Mg and Fe ( $[\text{M}/\text{H}] = -2.0$ ), but exhibit solar abundances for light elements such as C, N, O, and S (e.g., Hauck & Slettebak 1983; Gray 1988; Venn & Lambert 1990). Approximately 2% of the known A-stars in the field have been classified as  $\lambda$  Boo-type stars (Gray & Corbally 2002). On an HR diagram the  $\lambda$  Boo stars appear to lie between the zero-age and terminal age main sequences clouding the nature and evolutionary status of these stars (Paunzen & Gray 1997; Gray & Corbally 2002). Solano et al. (2001) provides an introduction into the competing theories for the nature of the  $\lambda$  Boo stars, briefly summarized here.

The first hypothesis is that  $\lambda$  Boo stars are young main sequence stars which are still surrounded by a shell or disk of gas and dust (Venn & Lambert 1990). The heavy, refractory elements are locked within the surrounding dust grains. The volatile elements remain in the gas and accrete onto the star, while the dust grains are blown away by the stellar radiation pressure taking the heavy elements with them, requiring the presence of circumstellar dust. All four of the known  $\lambda$  Boo stars within 40 pc have detected infrared excesses (Gray & Corbally 2002; Jura et al. 2005; Rieke et al. 2005; Chen et al. 2006) indicative of circumstellar dust. A continual accretion of the light gases at a rate of  $\approx 10^{-13} M_\odot \text{ yr}^{-1}$  (Charbonneau 1993) is needed. Once the accretion stops, the observed metal deficiencies fade within a million years. It is unclear if the surrounding disks contain enough light element gases to sustain the needed accretion rate over the main sequence lifetime of the star.

In this model,  $\lambda$  Boo stars would be relatively young (tens to hundreds of MYr) with solar-metallicity but with metal-deficient photospheres. Gray & Corbally (1998) obtained spectra of 60 Herbig Ae and pre-main sequence A-stars, which, in this scenario, would be expected to contain a higher fraction of  $\lambda$  Boo stars than the general field, but found only one  $\lambda$  Boo star and one marginal  $\lambda$  Boo star, a rate comparable to the field star rate.

A variation of this hypothesis places the  $\lambda$  Boo stars at the end of their main sequence lifetimes, and the shell is the result of mass loss. After  $10^9$  years of mass loss, diffusion in the atmosphere produces underabundances of the heavier elements (Michaud & Charland 1986). However, it is not clear if this mechanism can produce the strong underabundances of heavy elements that is observed in the  $\lambda$  Boo stars. In this hypothesis,  $\lambda$  Boo stars would be relatively old (a few GYr). At these ages, the  $\lambda$  Boo stars may be intrinsically more metal-poor than comparable A-stars which are younger.

Interestingly, Paunzen et al. (2002) concluded that the field  $\lambda$  Boo stars are located relatively homogeneously throughout their main sequence evolution. Based upon comparison to solar-metallicity isochrones, they find a uniform distribution of ages for  $\lambda$  Boo stars between 10 Myr to 500 Myr. This is followed by a rise in the number of  $\lambda$  Boo stars at an age of 0.6-1 Gyr, at which point the fraction of  $\lambda$  Boo stars relative to normal A-stars is higher than at younger ages.

An alternative hypothesis is that  $\lambda$  Boo stars are binary stars with both stars being of similar spectral type. The composite spectrum produces an apparent under-abundance of heavy elements (e.g., Faraggiana & Bonifacio 1999; Gerbaldi, Faraggiana, & Lai 2003). A complementary proposal is that  $\lambda$  Boo stars are actually contact binary stars (Andrievsky 1997). The composite colors of the star would look normal, but the spectral abundances would appear “metal-poor” (Faraggiana & Bonifacio 2005).

Nearly all of the work on  $\lambda$  Boo stars has involved detailed color and/or spectral analysis of the stars to determine effective temperatures, surface gravities, and elemental abundances. Determinations of basic stellar parameters, such as the stellar radii and masses, have been made indirectly from photometric fitting and comparison to evolutionary models. Optical interferometry, which is capable of resolving the stellar disk can add crucial and independent information to the debate on  $\lambda$  Boo stars.

We have made the first direct measurements of the angular diameter of the prototype for the class,  $\lambda$  Boötis (HD 125162, A3 V kB9.5mB9.5; Gray et al. 2003), using the Georgia State University’s (GSU) Center for High Angular Resolution Astronomy (CHARA) Array and the Palomar Testbed Interferometer (PTI). The CHARA Array with its long baselines (200 – 300 m) is uniquely suited for observations of absolute diameters of main sequence

stars, thereby, providing a unique perspective on the evolutionary status of  $\lambda$  Boo.

## 2. Observations and Data Reduction

$\lambda$  Boo was observed, in conjunction with two calibration stars, with the CHARA Array at  $2.2 \mu\text{m}$  on 4 nights between 2004 Jun 17 and 2004 Jun 29, utilizing the W1-E1 and E1-S1 baselines. It was then observed two years later on 2006 Jun 29 and 2006 Jun 30 with the E1-S1 baseline at  $1.67 \mu\text{m}$ .  $\lambda$  Boo, along with the calibration stars HD 125349 and HD 129002, was observed multiple times during each of these nights, and each observation, or scan, was approximately 200 s long. Observations of both calibrators bracketed each observation of  $\lambda$  Boo.

For each scan, we computed a mean  $V^2$ -value from the scan data, and the error in the  $V^2$  estimate from the rms internal scatter (ten Brummelaar et al. 2005).  $\lambda$  Boo was always observed in combination with its calibration sources HD 125349 and HD 129002. The calibrators (see Table 1) are expected to be unresolved by the interferometer with estimated angular sizes of  $0.198 \pm 0.012 \text{ mas}$  and  $0.286 \pm 0.018 \text{ mas}$ , respectively. These angular size estimates were based upon fitting template spectral energy distributions (SED) of the proper spectral type from Pickles (1998) to available broadband photometry available from IRSA<sup>1</sup> and SIMBAD. These objects were additionally selected to be slow apparent rotators, with  $v \sin i < 30 \text{ km s}^{-1}$  to ensure the stars are circularly symmetric (Uesugi & Fukuda 1982; Henry et al. 2000).

The calibration of the  $\lambda$  Boo  $V^2$  data is performed by estimating the interferometer system visibility ( $V_{sys}^2$ ) using the calibration source with model angular diameters and then normalizing the raw  $\lambda$  Boo visibility by  $V_{sys}^2$  to estimate the  $V^2$  measured by an ideal interferometer at that epoch (Mozurkewich et al. 1991; Boden et al. 1998). Uncertainties in the system visibility and the calibrated target visibility are inferred from internal scatter among the data in a scan and standard error-propagation calculations. More detail on the CHARA target and calibrator selection, data reduction, and technical aspects for the CHARA Array is available in the literature (McAlister et al. 2005; ten Brummelaar et al. 2005; van Belle et al. 2006).

In addition to the CHARA Array data, observations of  $\lambda$  Boo were obtained from the Palomar Testbed Interferometer (PTI; Colavita 1999) archive<sup>2</sup>.  $\lambda$  Boo was observed with

---

<sup>1</sup>NASA's Infrared Science Archive

<sup>2</sup>The archive is available at the Michelson Science Center (<http://msc.caltech.edu>).

PTI in 2000, 2003, and 2004 with the N-S, N-W, and S-W baselines (85-100 m) at both K and H bands. The PTI observations utilized the same calibrators as the CHARA observations.

Keeping the CHARA and PTI data separate, the data were grouped by baseline. The CHARA data were binned such that the bin widths were  $< 2\%$  of the central baseline length. The PTI data were binned by baseline configuration (e.g., N-S) and by wavelength (K-band vs. H-band). For each bin, the mean baseline lengths, position angles, and effective wavelengths were calculated, weighted by the quality of the  $V^2$  measurements. An error-weighted mean  $V^2$  was calculated for each bin. The resulting data are presented in Table 2, and the resulting visibility plot is shown in Figure 1.

### 3. Discussion

The primary result of this paper is the measurement of the apparent angular diameter for  $\lambda$  Boo. In the following sections, we discuss the angular diameter determination and the associated linear radius of  $\lambda$  Boo. We then relate these measurements to the effective temperature and mass, comparing  $\lambda$  Boo to other A-stars.

#### 3.1. Angular Diameter

We have modelled the observed mean visibilities as listed in Table 2 with a uniform disk of angular size  $\Theta_{UD}$  of the form:

$$V^2 = \left[ \frac{2J_1(\pi\Theta_{UD}(B/\lambda))}{\pi\Theta_{UD}(B/\lambda)} \right]^2 \quad (1)$$

where  $J_1$  is the first order Bessel function,  $B$  is the projected baseline length,  $\lambda$  is the wavelength of the observations, and  $\Theta_{UD}$  is the apparent uniform disk angular diameter. The best fit uniform disk diameter was found to be  $\Theta_{UD} = 0.527 \pm 0.028$  mas, ( $\chi^2_\nu \sim 0.4$ ).

Limb darkening in A stars in the near-infrared is expected to be relatively low (e.g. Claret, Díaz-Cordovés, & Giménez 1995); however, assuming that the star is a simple uniform disk will cause an underestimation of the true, limb-darkened disk size of the star by approximately 1%. Assuming a linear limb darkening law, the visibility function for a linear limb darkened stellar disk model can be parameterized as:

$$V^2 = \left[ \frac{1 - \mu_\lambda}{2} + \frac{\mu_\lambda}{3} \right]^{-2} \left[ \frac{(1 - \mu_\lambda)J_1[\pi(B/\lambda)\Theta_{LD}]}{\pi(B/\lambda)\Theta_{LD}} + \frac{(\mu_\lambda)j_1[\pi(B/\lambda)\Theta_{LD}]}{\pi(B/\lambda)\Theta_{LD}} \right]^2 \quad (2)$$

where  $\mu_\lambda$  is the linear limb darkening coefficient ( $\mu \approx 0.16$  for  $\lambda$  Boo; Claret, Díaz-Cordovés, & Giménez (1995)),  $j_1$  is the first order spherical Bessel function, and  $\Theta_{LD}$  is the apparent stellar limb darkened disk angular diameter (Hanbury Brown et al. 1974). The limb-darkening in the infrared for A-stars is sufficiently small that a large change in  $\mu_\lambda$  (25%) results in a very small change in the derived angular diameter ( $\lesssim 0.5\%$ ). The best fit limb darkened stellar disk diameter was determined to be  $\Theta_{LD} = 0.533 \pm 0.029$  mas. In Figure 1, we present the visibility curve for  $\lambda$  Boo with the best fit limb-darkened stellar disk model overlayed, along with the  $1\text{-}\sigma$  model fitting boundaries.

The measured angular diameter is in agreement with the angular diameter as predicted from interferometrically calibrated radius-color relationships for single stars ( $\Theta_{predict} \approx 0.54 - 0.56$  mas; van Belle 1999; Kervella et al. 2004). Speckle observations of  $\lambda$  Boo (McAlister et al. 1989) detected no companion brighter than  $\Delta m \lesssim 2$  mag, with a minimum separation of  $0''.03$  ( $30$  mas  $\approx 1$  AU at the distance of  $\lambda$  Boo). Further, Hipparcos observations of  $\lambda$  Boo display no signatures of a companion star or higher-order acceleration terms in the parallax solutions (Perryman 1997). Finally, the interferometric data presented here, spanning of nearly six years, are all consistent with a single-star model (see Figure 1).

The interferometric data do not represent a definitive null result for the existence of a companion star to  $\lambda$  Boo. However, if  $\lambda$  Boo contains an unrecognized (i.e., unknowingly detected) binary companion ( $\Delta K \gtrsim 1.5 - 2$ ), the presence of a companion in the interferometric data would *lower* the observed visibility amplitudes (as compared to a single star) and lead to an *over-estimation* of the stellar angular diameter. That, in turn, would imply that the true stellar radius is *smaller* than observed. Thus, the single-star assumption leads to an upper limit (within the measurement uncertainties) of the stellar radius.

### 3.2. Radius and Mass

The parallax of  $\lambda$  Boo, as measured by Hipparcos, is  $\pi = 33.58 \pm 0.61$  mas ( $d = 29.78_{-0.53}^{+0.55}$  pc; Perryman 1997; Heiter, Weiss, & Paunzen 2002). Taking the limb darkened stellar radius as the Rosseland (photospheric) angular diameter, we derive a linear radius for  $\lambda$  Boo of  $R_\star = 1.70 \pm 0.10 R_\odot$ .

If we combine the linear radius with a surface gravity, we can derive an estimate for the mass of  $\lambda$  Boo. Castelli & Kurucz (2001) fit the IUE spectrum of  $\lambda$  Boo with an atmosphere model that is metal-poor in all the heavy elements ( $[M/H] = 0.0$ ) except for C, N, & O. They found the best fit model to have a temperature of 8500-8600 K and a surface gravity of

$\log(g) = 4.0$  [ $\text{cm s}^{-2}$ ]. They note that Breger (1976), by fitting to only the visible part of the spectrum, determined a best fit temperature and surface gravity of 8550 K and  $\log(g) = 4.1$  [ $\text{cm s}^{-2}$ ]. Using photometric relationships, Chen et al. (2006) derive a surface gravity of  $\log(g) = 4.198$  [ $\text{cm s}^{-2}$ ].

From this surface gravity range, we infer a stellar mass range for  $\lambda$  Boo of  $M_\star = 1.1 - 1.7 M_\odot$ . For a given surface gravity, the linear radius uncertainty contributes approximately  $\sigma(M_\star) = 0.1 - 0.2 M_\odot$  to the total mass uncertainty. Thus, the uncertainty in the mass (i.e., the range of masses derived) is primarily a result of the uncertainty in the surface gravity.

In comparison, we have derived the masses for  $\beta$  Leo (A3V), Sirius (A1V), and Vega (A0V), three well-studied early A-type main sequence stars that have had their diameters measured directly. Of these three A-stars,  $\beta$  Leo is the closest to  $\lambda$  Boo in spectral type (A3V *vs.* A3V kB9.5mB9.5), and provides the best comparison to  $\lambda$  Boo.

$\beta$  Leo and Sirius have limb darkened angular diameters of  $\Theta_{\beta\text{Leo}} = 1.45 \pm 0.03$  mas (Di Folco et al. 2004) and  $\Theta_{\text{Sirius}} = 6.01 \pm 0.02$  mas (Kervella et al. 2003). Combined with the parallaxes ( $\pi = 90.16 \pm 0.89$  &  $379.21 \pm 1.58$  mas), we derive linear radii of  $R_{\beta\text{Leo}} = 1.72 \pm 0.04 R_\odot$  and  $R_{\text{Sirius}} = 1.71 \pm 0.01 R_\odot$  – very similar to the radius measured for  $\lambda$  Boo. With respective surface gravities of  $\log(g) = 4.26$  [ $\text{cm s}^{-2}$ ] (Erspamer & North 2003) and  $\log(g) = 4.31$  [ $\text{cm s}^{-2}$ ] (Sadakane & Ueta 1989), the derived masses of  $\beta$  Leo and Sirius are  $M_{\beta\text{Leo}} = 1.97 \pm 0.09 M_\odot$  and  $M_{\text{Sirius}} = 2.01 \pm 0.05 M_\odot$ . Vega is larger ( $R \approx 2.5 R_\odot$ ) and more massive ( $M_{\text{Vega}} = 2.3 \pm 0.2 M_\odot$ ) than  $\lambda$  Boo,  $\beta$  Leo, and Sirius (Aufdenberg et al. 2006).

The distribution of derived stellar mass as a function of surface gravity for  $\lambda$  Boo is shown in Figure 3. The figure demonstrates that the mass for  $\lambda$  Boo is in rough agreement (within  $1\sigma$ ) with the mass of  $\beta$  Leo and Sirius if the surface gravity for  $\lambda$  Boo is  $\log(g) \approx 4.2$ . If the surface gravity is nearer to  $\log(g) = 4.0$  or  $\log(g) = 4.1$  as indicated by the detailed UV and optical spectral fitting, then the derived mass for  $\lambda$  Boo is  $2 - 3\sigma$  below that found for the three young A-stars  $\beta$  Leo, Sirius, and Vega.

We note here that the known debris disk surrounding Vega was likely detected with the interferometric observations at PTI (Ciardi et al. 2001) and independently with observations at the CHARA Array (Absil et al. 2006).  $\lambda$  Boo has a stronger mid-infrared excess than Vega, indicative of circumstellar material surrounding the star which is the primary reason for the conjectured association of  $\lambda$  Boo stars with Vega-like stars (e.g., Jura et al. 2005; Rieke et al. 2005; Chen et al. 2006). There is no evidence in our data that the circumstellar material has been detected by the CHARA Array. However, *if* the surrounding shell and/or disk indeed had been detected, the circumstellar material would serve to make  $\lambda$  Boo appear *larger* than it actually is, yielding an upper limit to the stellar radius and mass.

### 3.3. Evolutionary Status and Age

Previous estimates of the mass of  $\lambda$  Boo have been made by placing it on a luminosity-temperature HR diagram (Iliev & Barzova 1995; Paunzen 1997; Paunzen et al. 2002) and comparing its position to that of solar-metallicity stellar evolutionary models (Schaller et al. 1992; Claret 1995; Morel 1997). These works report a  $\lambda$  Boo effective temperature range of  $T_{eff} \approx 8600\text{--}8900$  K and a luminosity range of  $L_{\star} \approx 15\text{--}24 L_{\odot}$  (see Table 4 in Paunzen et al. (2002) for a summary). The inferred mass range, from comparison to the solar metallicity stellar evolutionary models, of these works is  $M_{\star} \approx 2.0\text{--}2.1 M_{\odot}$ . We wish to place  $\lambda$  Boo on a luminosity-temperature HR diagram to explore the differences between our *derived* mass for  $\lambda$  Boo and the *inferred* mass by previous works.

The measured angular diameter allows us to derive the effective temperature of  $\lambda$  Boo via the Stefan-Boltzmann equation:

$$T_{eff} = \left[ \frac{L_{\star}}{4\pi\sigma R_{\star}^2} \right]^{1/4} = \left[ \frac{F_{bol} D_{\star}^2}{\sigma R_{\star}^2} \right]^{1/4} \quad (3)$$

where  $L_{\star}$  is the luminosity,  $R_{\star}$  is the stellar radius,  $\sigma$  is the Stefan-Boltzmann constant,  $F_{bol}$  is the bolometric flux and  $D_{\star}$  is the distance to the star. In terms of the angular diameter in milli-arcsec ( $\Theta$ ) and in units of  $10^{-10}$  W m $^{-2}$  for  $F_{bol}$ , equation (3) may be written as

$$T_{eff} = 4163 \left[ \frac{F_{bol}}{\Theta^2} \right]^{1/4}. \quad (4)$$

The bolometric flux for  $\lambda$  Boo was estimated by fitting the ultra-violet (IUE) to near-infrared (2MASS) spectral energy distribution with templates from Lejeune et al. (1997) (Figure 2). The bolometric flux is  $F_{bol} = 5.901 \pm 0.041 \times 10^{-10}$  W m $^{-2}$ . At a distance of  $d = 29.78_{-0.53}^{+0.55}$  pc, this corresponds to a luminosity of  $L_{\star} = 16.3 \pm 0.6 L_{\odot}$ . Combined with the limb darkened angular diameter, we derive an effective temperature of  $T_{eff} = 8887 \pm 242$  K. Our temperature estimate is in good agreement with temperatures reported in the literature which range from 8550 K (Castelli & Kurucz 2001) to 8920 K (Holweger, Hempel, & Kamp 1999).

Using the interpolator provided with the the Yonsei-Yale ( $Y^2$ ) stellar evolutionary models (Demarque et al. 2004), we have generated isochrones and evolutionary tracks for solar metallicity ( $z=0.02$ ,  $[M/H] \approx 0.0$ ) and sub-solar metallicity ( $z=0.0002$ ,  $[M/H] \approx -2.0$ ). For the mass tracks, the stellar masses span  $0.8\text{--}2.7 M_{\odot}$  in steps of  $0.1 M_{\odot}$ , evolved across both the pre-main sequence and post-main sequence. The HR diagrams, in terms of stellar luminosity vs. effective temperature as represented by the  $Y^2$  models, are shown in Figure



4. The position of  $\lambda$  Boo, as measured by the interferometers, is marked in each of the HR diagrams.

The position of  $\lambda$  Boo on the solar-metallicity diagram (*top* Figure 4) implies that  $\lambda$  Boo should have a stellar mass of  $M_{\star} = 1.9 - 2.1 M_{\odot}$ , in agreement with the upper bound derived for the mass of  $\lambda$  Boo ( $\log(g) = 4.2$ ,  $M_{\star} = 1.7 \pm 0.2 M_{\odot}$ ). If  $\lambda$  Boo is represented by the solar metallicity models, the star is fairly young with an age of  $8 - 300$  Myr. This age would be consistent with  $\lambda$  Boo being related to the Vega-like stars (i.e., stars with dusty debris disks), but being younger than Vega itself (Jura et al. 2005; Rieke et al. 2005).

In contrast, placing  $\lambda$  Boo on a set of sub-solar metallicity models (*bottom* Figure 4), the (post)-main sequence models imply a stellar mass of  $M_{\star} = 1.2 - 1.4 M_{\odot}$ , in agreement with the mid-range for the mass derived from our observations ( $\log(g) = 4.1$ ,  $M_{\star} = 1.3 \pm 0.2 M_{\odot}$ ). The pre-main sequence tracks imply a slightly larger stellar mass of  $M_{\star} = 1.5 - 1.6 M_{\odot}$ .

The ages associated with the sub-solar metallicity pre- and post-main sequence tracks are quite different from each other. For these models, if  $\lambda$  Boo is a pre-main sequence star, it would need to be extremely young ( $3 - 4$  Myr). At such a young age, the star should be associated with the Herbig AeBe (HAeBe) stars. Yet,  $\lambda$  Boo shows no Balmer emission lines (e.g., Iliev & Barzova 1998), an observational requirement of the HAeBe stars (Thé et al. 1994). Additionally, at a galactic position of  $l = 86^{\circ}$ ,  $b = 65^{\circ}$ ,  $d = 29.8$  pc,  $\lambda$  Boo is not directly associated with any molecular clouds or regions of high extinction (Lucke 1978; Gaustad & van Buren 1993). These discrepancies suggest that  $\lambda$  Boo, if best described by the sub-solar metallicity evolutionary tracks, is not  $3 - 4$  Myr old.

If  $\lambda$  Boo is a post-main sequence star, the sub-solar metallicity models place it at an age of  $2 - 3$  Gyr, and the star is at (or past) the terminal age for the main sequence. We note here that this independent assessment of the age of  $\lambda$  Boo is in general agreement with the results of Paunzen et al. (2002) who found that the  $\lambda$  Boo stars span an age range of 10 Myr to 1.5 Gyr with a strong peak near 1.0 Gyr.

#### 4. Summary

We have presented the first direct determination of the angular size of the chemically peculiar star  $\lambda$  Boötis. The infrared interferometric observations made use of the longest baselines on the CHARA Array and the Palomar Testbed Interferometer. The primary result of this work is the direct determination of the limb darkened angular diameter of  $\lambda$  Boo, which was measured to be  $\Theta_{LD} = 0.533 \pm 0.029$  mas. A full summary of the stellar parameters derived from the spatially resolved interferometric observations are presented in

Table 3.

In combining our independently determined stellar radius with previous determinations of the surface gravity, we have calculated a stellar mass range for  $\lambda$  Boo of  $M_{\star} = 1.1 - 1.7 M_{\odot}$ . The radius determination contributes  $0.1 - 0.2 M_{\odot}$  to the uncertainty. The remainder of the mass uncertainty is contributed entirely by the uncertainty in surface gravity ( $\log(g) = 4.0 - 4.2$ ).

Solar-metallicity ( $z=0.02$ ,  $[M/H] \approx 0.0$ ) stellar evolutionary models predict that  $\lambda$  Boo should have a mass nearer to  $1.9 - 2.1 M_{\odot}$ , in agreement with the upper bound of our mass determination ( $\log(g) = 4.2$ ,  $M_{\star} = 1.7 \pm 0.2 M_{\odot}$ ). Metal-poor ( $z=0.0002$ ,  $[M/H] \approx -2.0$ ) stellar evolutionary models predict a mass  $1.2 - 1.4 M_{\odot}$  in agreement with the mid-range of our interferometrically derived mass ( $\log(g) = 4.1$ ,  $M_{\star} = 1.3 \pm 0.2 M_{\odot}$ ). A more definitive surface gravity determination is required to distinguish between these two sets of models.

The authors would like to thank the entire staff at the CHARA Array for without them this work would not have been possible. Portions of this work were performed at the California Institute of Technology under contract with the National Aeronautics and Space Administration. This research has been supported by National Science Foundation grants AST-0307562 and AST-0606958 to Georgia State University. Additional support has been received from the Research Program Enhancement program administered by the Vice President for Research at Georgia State University. Work done with the Palomar Testbed Interferometer was performed at the Michelson Science Center, California Institute of Technology, under contract with the National Aeronautics and Space Administration. Interferometer data were obtained at Palomar Observatory using the NASA PTI, supported by NASA contracts to the Jet Propulsion Laboratory. Science operations with PTI are conducted through the efforts of the PTI Collaboration, and we acknowledge the invaluable contributions of our PTI colleagues.

This research has made use of the NASA/IPAC Infrared Science Archive, which is operated by the Jet Propulsion Laboratory, California Institute of Technology, under contract with the National Aeronautics and Space Administration. This research has made use of data obtained from the High Energy Astrophysics Science Archive Research Center (HEASARC), provided by NASA’s Goddard Space Flight Center. This research has made use of the SIMBAD database, operated at CDS, Strasbourg, France.

## REFERENCES

- Absil, O., et al. 2006, *A&A*, 452, 237
- Andrievsky, S. M. 1997, *A&A*, 321, 838
- Aufdenberg, J. P., et al. 2006, *ApJ*, 645, 664
- Baschek, B. & Searle, L. 1969, *ApJ*, 155, 537
- Boden, A.F, et al., 1998, *ApJ*, 504, L39
- Breger, M. 1976, *ApJS*, 32, 7
- Castelli, F., & Kurucz, R. L. 1994, *A&A*, 281, 817
- Castelli, F., & Kurucz, R. L. 2001, *A&A*, 372, 260
- Charbonneau, P. 1993, *ApJ*, 405, 720
- Chen, C. H. et al. 2006, *ApJS*, 166, 351
- Ciardi, D. R., et al. 2001, *ApJ*, 559, 1147
- Claret, A. 1995, *A&AS*, 109, 441
- Claret, A., Díaz-Cordovés, J., & Giménez, A. 1995, *A&A*, 114, 247
- Colavita, M. M. et al. 1999, *ApJ*, 510, 505
- Cowley, A., Cowley, C., Jaschek, M., & Jaschek, C. 1969, *AJ*, 74, 375
- Demarque, P., Woo, J.-H., Kim, Y.-C., & Yi, S. K. 2004, *ApJS*, 155, 667
- Di Folco, E., Thévenin, F., Kervella, P., Domiciano de Souza, A., Coudé du Foresto, V., Ségransan, D., & Morel, P. 2004, *A&A*, 426, 601
- Erspamer, D., & North, P. 2003, *A&A*398, 1121
- Faraggiana, R. & Bonifacio, P. 1999, *A&A*, 349, 521
- Faraggiana, R. & Bonifacio, P. 2005, *A&A*, 436, 697
- Gaustad, J. E., & van Buren, D. 1993, *PASP*, 105, 1127
- Gerbaldi, M., Faraggiana, R., & Lai, O. 2003, *A&A*, 412, 447

- Gray, R. O. 1988, AJ, 95, 220
- Gray, R. O. & Corbally, C. J. 1998, AJ, 116, 2993
- Gray, R. O. & Corbally, C. J. 2002, ApJ, 124, 989
- Gray, R. O., Corbally, C. J., Garrison, R. F., McFadden, M. T., & Robinson, P. E. 2003, AJ, 126, 2048
- Hanbury Brown, R., Davis, J., Lake, R. J. W., & Thompson, R. J. 1974, MNRAS, 167, 475
- Hauck, B., & Slettebak, A. 1983, A&A, 127, 231
- Heiter, U., Weiss, W. W., & Paunzen, E., 2002, A&A, 381, 971
- Henry, G. W., Fekel, F. C., Henry, S. M., & Hall, D. S. 2000, ApJS, 130, 201
- Holweger, H., Hempel, M. & Kamp, I. 1999, A&A, 350, 603
- Iliev, I. Kh. & Barzova, I. S. 1995, A&A, 302, 735
- Iliev, I. K., & Barzova, S. I. 1998, Contributions of the Astronomical Observatory Skalnaté Pleso, 27, 441
- Kervella, P., Thévenin, F., Morel, P., Bordé, P., & Di Folco, E. 2003, A&A, 408, 681
- Kervella, P., Thévenin, F., Di Folco, E., & Ségransan, D. 2004, A&A, 426, 297
- Jura, M. et al. 2005, ApJS, 153, 453
- Lejeune, T., Cuisinier, F., & Buser, R. 1997, A&AS, 125, 229
- Lucke, P. B. 1978, A&A, 64, 367
- McAlister, H.A., et al. 1989, AJ, 97, 510
- McAlister, H.A., et al. 2005, ApJ, 628, 439
- Michaud, G. & Charland, Y. 1986, ApJ, 311, 326
- Morel, P. 1997, A&AS, 124, 597
- Morgan, W.W., Keenan, P. C., & Kellman, E. 1943, An Atlas of Stellar Spectra (University of Chicago Press)
- Mozurkewich, D., et al., 1991, AJ, 101, 2207

- Paunzen, E. 1997, *A&A*, 326, L29
- Paunzen, E. & Gray, R. O. 1997, *A&AS*, 126, 407
- Paunzen, E., Iliev, I. Kh., Kamp, I., & Barzova, I. S. 2002, *MNRAS*, 336, 1030
- Perryman, M. A. C. 1997, The HIPPARCOS and TYCHO catalogues. Astrometric and photometric star catalogues derived from the ESA HIPPARCOS Space Astrometry Mission (ESA SP Ser. 1200)
- Pickles, A. J. 1998, *PASP*, 110, 863
- Rieke, G. H. et al. 2005, *ApJ*, 620, 1010
- Sadakane, K., & Ueta, M. 1989, *PASJ*, 41, 279
- Schaller, G., Schaerer, D., Meynet, G., & Maeder, A. 1992, *A&AS*, 96, 269
- Solano, E., Paunzen, E., Pintado, O. I., & Varela, J. 2001, *A&A*, 374, 957
- Slettebak, A. 1954, *ApJ*, 119, 146
- ten Brummelaar, T., et al., 2005, *ApJ*, 628, 453
- Thé, P. S., de Winter, D., & Perez, M. R. 1994, *A&AS*, 104, 315
- Uesugi, A., Fukuda, I., 1982, Revised Catalogue of Stellar Rotational Velocities
- van Belle, G. T. 1999, *PASP*, 11, 1515
- van Belle, G. T., et al. 2006, *ApJ*, 637, 494
- Venn, K. A. & Lambert, D. L. 1990, *ApJ*, 363, 234

Table 1. Calibration Stars

Star	$\theta_{EST}^a$ (mas)	Distance from $\lambda$ Boo (deg)	Spectral Type
HD 129002	$0.198 \pm 0.012$	4.3	A1 V
HD 125349	$0.286 \pm 0.018$	5.3	A1 IV

<sup>a</sup>Estimated angular diameters derived from spectral energy distribution modeling.

Table 2. Weighted Mean Visibilities

Array	Number of Points in Average	Mean <sup>a</sup> Projected Baseline (m)	Mean <sup>a</sup> Position Angle E. of N. (deg)	Mean <sup>a</sup> Effective Wavelength ( $\mu$ m)	Mean <sup>b</sup> Normalized V <sup>2</sup>
CHARA	3	226.7 (3.7)	291.0 (1.1)	2.133	$0.803 \pm 0.057$
CHARA	4	241.0 (1.1)	295.6 (1.0)	2.133	$0.897 \pm 0.051$
CHARA	3	251.5 (1.8)	299.8 (0.8)	2.133	$0.753 \pm 0.050$
CHARA	3	258.6 (3.3)	303.3 (2.6)	2.133	$0.824 \pm 0.066$
CHARA	3	328.1 (2.0)	191.8 (4.0)	1.673	$0.573 \pm 0.081$
PTI	20	85.8 (0.9)	241.9 (7.7)	2.217 (0.005)	$0.999 \pm 0.020$
PTI	11	85.0 (1.0)	325.7 (7.6)	2.214 (0.002)	$0.962 \pm 0.036$
PTI	25	108.5 (0.6)	191.3 (6.6)	2.242 (0.008)	$0.965 \pm 0.040$
PTI	6	109.0 (0.1)	179.6 (6.1)	1.641 (0.001)	$0.911 \pm 0.040$

<sup>a</sup>Values in parentheses represent the rms dispersions.

<sup>b</sup>Uncertainties derived from the weighted mean.

Table 3.  $\lambda$  Boötis Stellar Properties

Parameter	Value Using		Units	Reference
	[M/H] = 0.0	[M/H] = -2.0		
Parallax	$33.58 \pm 0.61$		mas	5
Limb Darkened Diameter	$0.533 \pm 0.029$		mas	1
Linear Radius	$1.70 \pm 0.10$		$R_{\odot}$	1
$v \sin(i)$	$100 \pm 10$		$\text{km s}^{-1}$	4
Bolometric Flux	$5.901 \pm 0.041$		$10^{-10} \text{ W m}^{-2}$	1
Luminosity	$16.3 \pm 0.6$		$L_{\odot}$	1
Effective Temperature	$8887 \pm 242$		K	1
Surface Gravity	4.0 – 4.2		$\log [\text{cm s}^{-1}]$	2,3
Mass	1.1 – 1.7 <sup>a</sup>		$M_{\odot}$	1
Pre-MS Age	8 – 30	3 – 4	Myr	1
Post-MS Age	0.08 – 0.3	2 – 3	Gyr	1
Model Mass Range	1.9 – 2.0	1.3 – 1.6	$M_{\odot}$	1

<sup>a</sup>The radius uncertainty contributes approximately an uncertainty of 0.1-0.2  $M_{\odot}$  for a given value of the surface gravity. The range in mass represents the range in surface gravity.

References. — 1. This Work; 2. Castelli & Kurucz (2001); 3. Chen et al. (2006); 4. Heiter, Weiss, & Paunzen (2002); 5. Perryman (1997)

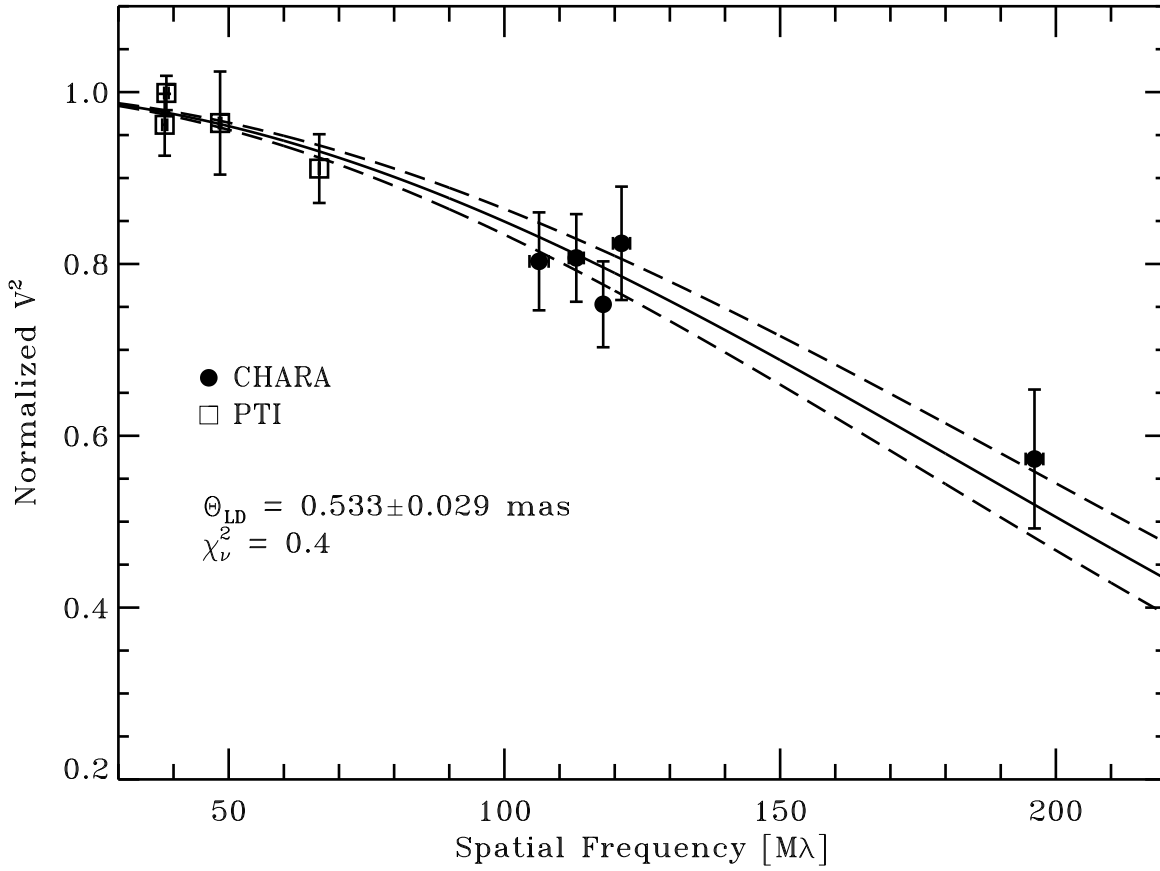


Fig. 1.— Normalized visibility vs. spatial frequency for  $\lambda$  Boo as listed in Table 2. Data obtained with the CHARA Array are shown with the filled circles; data obtained with PTI are shown with the open squares. Error bars represent  $1\text{-}\sigma$  uncertainties. The solid line represents the best-fit limb-darkened stellar disk model fit. The dashed lines represent the  $1\text{-}\sigma$  fitting uncertainties.



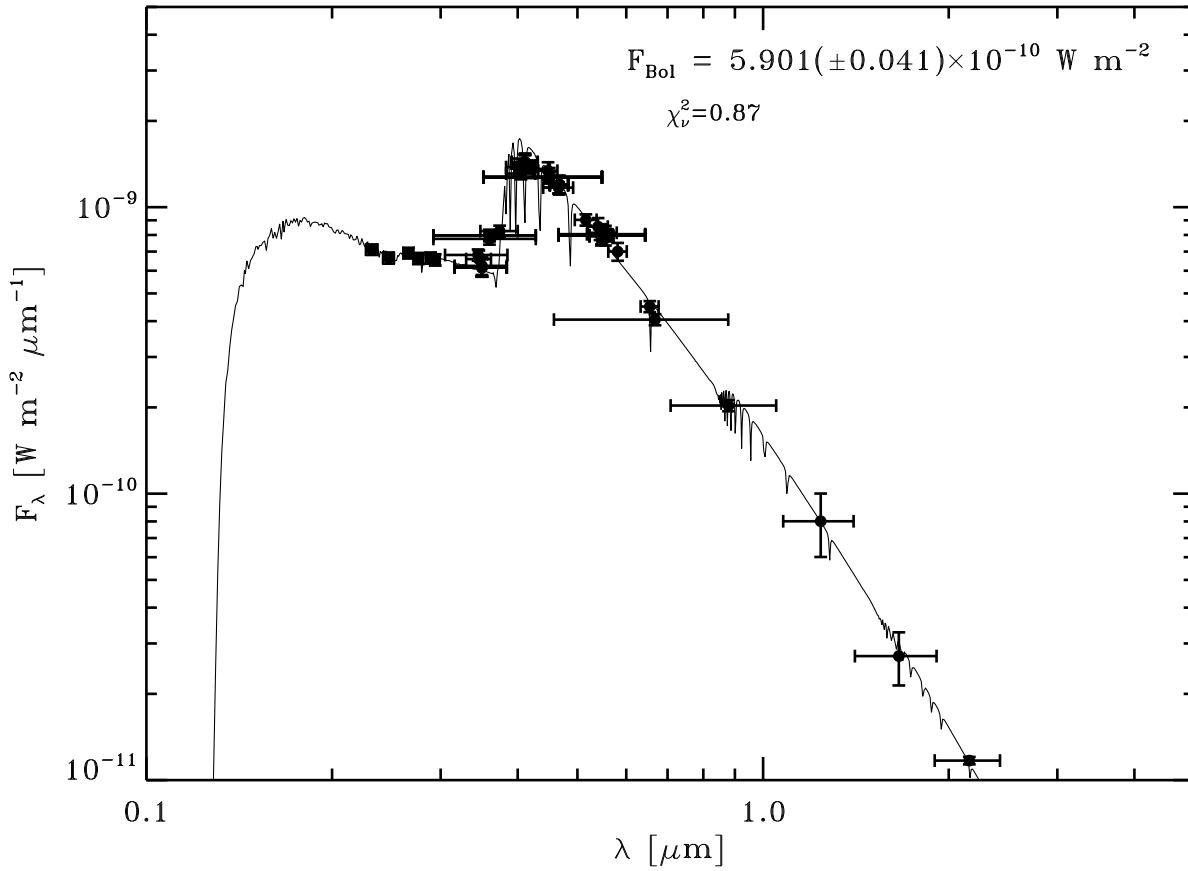


Fig. 2.— Model spectral energy distribution and flux density data for  $\lambda$  Boo. The horizontal error-bars represent the bandwidths associated with the observations. The data have been fit with a 8750 K  $[\text{M}/\text{H}] = -2.0$  template from Lejeune et al. (1997).

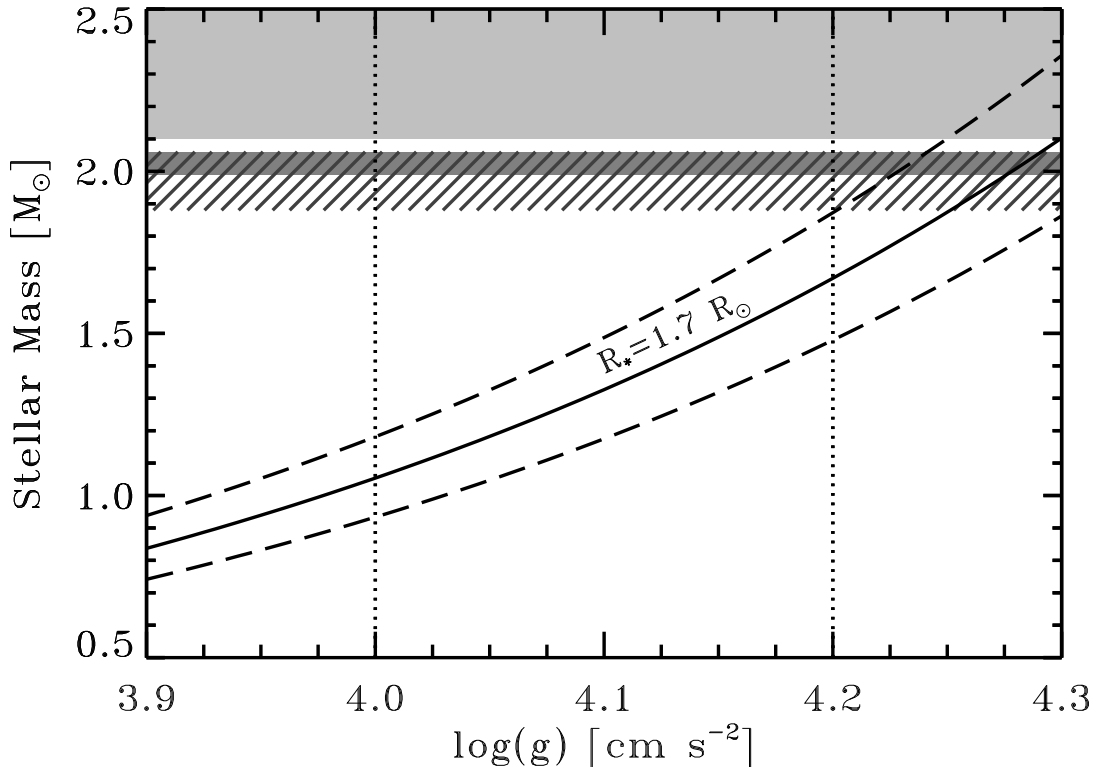


Fig. 3.— A plot of the derived stellar mass for  $\lambda$  Boo as a function of surface gravity. The solid line represents the linear radius ( $R_{\star} = 1.7 R_{\odot}$ ) as derived from the measured angular diameter. The dashed lines represent the  $1\sigma$  uncertainty limits for  $\lambda$  Boo. The vertical dotted lines delineate the range of surface gravity ( $\log(g) = 4.0 - 4.2$ ) for  $\lambda$  Boo, as discussed in the text. For comparison, the light gray region marks the derived mass of Vega; the dark gray region marks the derived mass for Sirius, and the hatched region marks the derived mass for  $\beta$  Leo.

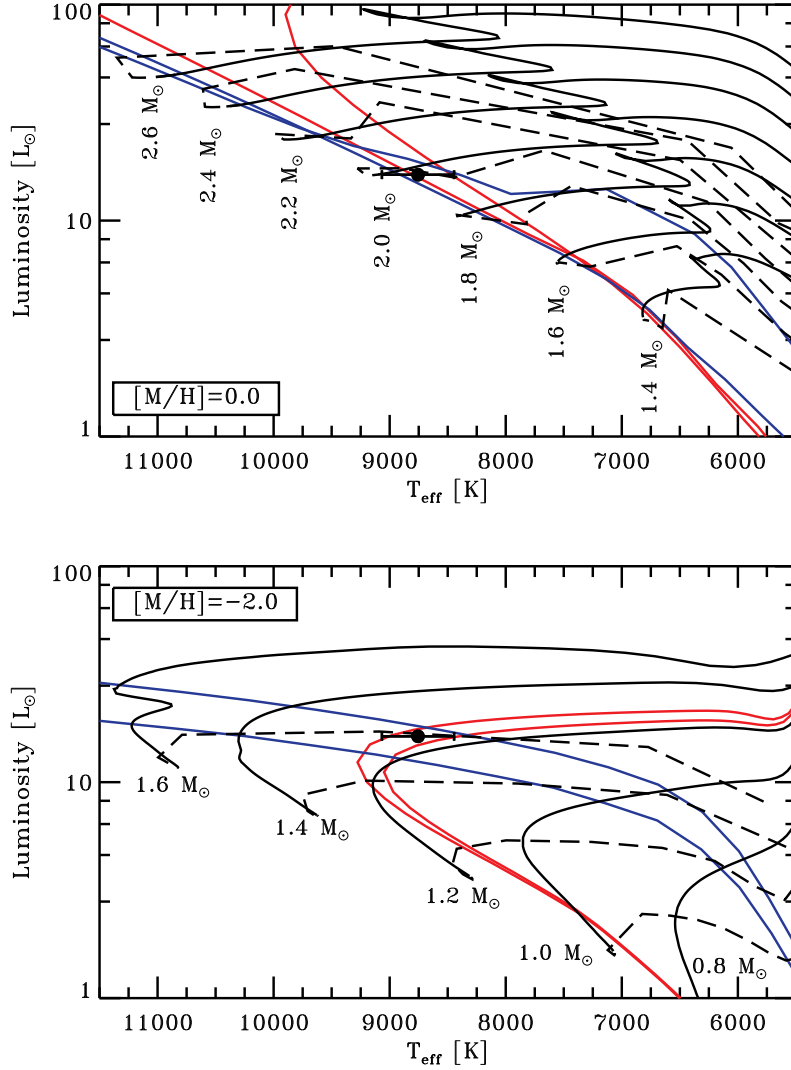


Fig. 4.— The derived linear radius and effective temperature for  $\lambda$  Boo are shown versus the pre-main sequence evolutionary tracks (dashed black lines) and (post-)main sequence evolutionary tracks (solid black lines) for the  $Y^2$  stellar evolutionary models. *Top*: Models for a metallicity of  $[M/H] \approx 0.0$ . *Bottom*: Models for a metallicity of  $[M/H] \approx -2.0$ . The stellar mass for each track is labelled in solar masses. The solid blue and solid red lines in each panel represent pre- and post-main sequence isochrones, respectively. For the solar metallicity models (*top*), the two pre-main sequence isochrones (blue) correspond to 8 Myr and 30 Myr, and the two post-main sequence isochrones (red) correspond to 80 Myr and 300 Myr. For the metal-poor models (*bottom*), the pre-main sequence (blue) and post-main sequence (red) isochrones correspond to 3 & 4 Myr and 2.6 & 2.8 Gyr, respectively.